JOURNAL OF CATALYSIS 126, 496–518 (1990)

Localization and Structure of Carbonaceous Deposits on Reforming Catalysts

D. ESPINAT,*,[1] E. FREUND,* H. DEXPERT,† AND G. MARTINO*

*Institut Français du Pétrole, Boîte Postale 311, 92506 Rueil Malmaison Cedex, France; and †Laboratoire pour l'Utilisation du Rayonnement Electromagnétique (LURE), Bât. 209 C, 91401 Orsay Cedex, France

Received December 30, 1988; revised May 15, 1990

The aging of alumina-supported Pt-containing reforming catalysts by "coke" deposition has previously been extensively investigated. In the present work, a large number of techniques including optical and electron microscopy have been used to determine both the localization and the structure of the so-called "coke" (carbonaceous deposits) formed during the normal operation of these catalysts. The coke is not uniformly deposited on the surface of the catalysts. Its structure is not uniform for a given catalyst, and depends on the operating conditions (especially the H_2/hydrocarbon ratio) as well as the composition of the metallic phase (pure platinum or multimetallic alloy). The structure is always rather well organized (pregraphitic) even at the onset of coke deposition.

1. INTRODUCTION

Catalytic reforming (*1*) is a process for transforming virgin naphtha into high-octane gasoline. For technical and economic reasons, it is advantageous to run the reforming unit under severe conditions, i.e., high temperatures and low hydrogen partial pressure, and accordingly, to maximize the yields of desirable products, especially aromatics. Catalyst stability thus becomes a very important parameter. The search for higher stabilities has led to the replacement of platinum-based catalysts by multimetallic catalysts, in which other elements such as rhenium, iridium, tin, and germanium are combined with platinum.

In principle, the deactivation of these catalysts can be related first to carbonaceous deposits, and secondly to sintering of the metal. Since it was previously shown (*2*) that the sintering of platinum is slow and is inhibited by chlorination of the carrier and the addition of other metals, it is apparent that coke formation plays a determining role in catalyst deactivation.

It is generally assumed that coke is formed from highly dehydrogenated molecules, the reaction occurring either at the catalyst surface or in the gas phase (*3–6*). The precise location of the coke on the metal or carrier has not been established. However, both acidic and metallic catalyst activities are affected by coke formation (*7–10*). Information related to the coke structure indicates the presence of both amorphous and organized carbon (*11–13*). This work aims to describe two important features of the coke deposit, namely its localization and structure (*14*).

After evaluating the effects of coke deposits on the catalytic functions, we first consider a global description, at the scale of one or more pellets, by determining the overall surface area and porosity using optical microscopy and ion or electron microprobes (these methods allow a quantitative evaluation of the distribution inside the pellets). To obtain higher spatial resolution, we used both conventional and scan-

[1] Author to whom correspondence should be addressed.

0021-9517/90 $3.00

ning transmission electron microscopy (CTEM and STEM, respectively).

As to the structural characterization of coke, both X-ray and electron diffraction are applied, either to the catalysts as such, or to the coke isolated after selective dissolution of the alumina carrier by dilute hydrofluoric acid under controlled conditions. Raman laser spectroscopy (*13*) also proved to be very effective for characterizing the coke, even at very low carbon content.

TABLE 1

Preparation of Bimetallic Catalysts

Catalyst	Precursor for second metal	Reference
Pt–Ir	H_2IrCl_6	(*15*)
Pt–In	$InCl_3$	(*16*)
Pt–Ge	germanium oxalate	(*17*)
Pt–Sn	$SnCl_2$	(*18*)
Pt–Re	ammonium perrhenate	(*19*)

2. EXPERIMENTAL

2.1. Preparation of Fresh Catalysts

Monometallic catalysts were prepared using hexachloroplatinic acid as the impregnating salt, in the presence of hydrochloric acid. The alumina support is a γ_c-alumina. The surface area is 234 $m^2\ g^{-1}$ and the pore volume equal to 0.64 $cm^3\ g^{-1}$. After impregnation, the catalyst precursor was dried, calcined in air at 703 K for 2 hr, and then reduced in pure flowing hydrogen at 573 K. It was again reduced in the catalyst test unit.

Two different techniques were used for preparation of the supported bimetallic catalysts, namely (i) co-impregnation of the two metallic precursors for the preparation of the Pt–Ir bimetallic catalyst, (ii) impregnation in two steps for the other fresh catalysts (Pt–In, Pt–Ge, Pt–Sn, Pt–Re), the platinum precursor being impregnated first.

Further information is given in Table 1.

2.2. Preparation of Coked Catalysts and Catalytic Testing

The coked catalyst samples were prepared (*20*) and catalytic tests carried out in the same apparatus. Two different tests were performed (see Table 2). Two purified feeds dried on molecular sieves (4A and 13X) were used according to the desired reaction with *n*-heptane or benzene/*n*-heptane. The working conditions were determined by temperature, flow rate, overall pressure, and H_2/hydrocarbon (HC) molar ratio. For isomerization/cracking, the catalysts were coked under condition 1 (Table 2) for variable periods. These conditions were more severe (higher temperature, lower H_2/HC ratio) than the test conditions, so that coking during the test could be neglected. Benzene hydrogenation was carried out after coking under condition 2.

The carbon content of a coked catalyst was determined by combustion under oxygen. The coke percentage is defined as the mass of carbon deposited for 100 g of fresh catalyst.

TABLE 2

Operating Conditions for Catalytic Tests of the Metallic and Acidic Functions

Test conditions	Reaction		Coking conditions	
	Isomerization cracking	Benzene hydrogenation	1	2
Temperature (K)	623	373	723	803
Overall pressure (MPa)	3.5	0.5	0.5	0.4
H_2/HC Molar ratio	14	23[b]	2	1
PPH[a] ($g\ g^{-1}\ hr^{-1}$)	3.5	1.5[c]	3.5	20
Feed	nC_7	nC_7 (87.4%) + C_6H_6 (12.6%)	nC_7	nC_7 (87.4%) + C_6H_6 (12.6%)

[a] PPH : g of feed injected per g of catalyst and per hour.
[b] HC = C_6H_6.
[c] HC/C_6H_6.

2.3. Determination of Surface Area and Pore Volume

Conventional methods (*21, 22*) were employed. The adsorption isotherm for N_2 at 77 K were measured using a Carlo Erba sorptometer. This allowed the determination of both the specific area (BET method) and the porosity, using two types of pore model (slit and cylindrical pores). High-pressure mercury porosimetry was also used to determine the porosity between 3.5 nm and 300 μm. Low-pressure mercury porosimetry gave the grain density (d_g, and helium pycnometry (*23*) gave the structural density (d_s), a very important parameter at high coke contents.

2.4. Selective Dissolution of Alumina Carrier

The alumina carrier was eliminated by dilute hydrofluoric acid. The carbonaceous deposits were found to be insoluble in this medium, and their structure is unaffected (*24*).

Large amounts of catalyst had to be treated for some experiments, in which we used (40 wt% HF) mixed with fuming (37 wt%) HCl at 60°C. Dilute 10 wt% HF was used for the electron microscopy samples.

2.5. X-Ray Diffraction

A Siemens D 501 automatic diffractometer was used, with a copper anticathode and a scintillation counter. The spectra were recorded using continuous rotation or a step-by-step procedure.

2.6. Electron Microprobe

The carbon concentrations along diameters in the equatorial sections of the catalyst pellets or spheres were obtained with a Camebax electron microprobe. Due to low sensitivity, long counting times were necessary (spatial resolution 5 μm).

2.7. Ion Microprobe (SIMS)

The analyses were made with an IMS 3F SIMS (Cameca) instrument. Sample preparation was identical to that for the electron microprobe. O_2^+ ions were selected as primary ions. A 10-μm spatial resolution could be reached with high sensitivity.

2.8. Optical Microscopy

A Polyvar-Met microscope was used (Reichert Jung). The samples were first crushed in ethanol. Some drops of the suspension were deposited and evaporated on a glass. Observations were made in reflection mode.

2.9. Electron Microscopy

The following measurements were taken.

Normal imaging mode: both a JEOL 120 CX Conventional Transmission Electron Microscope (CTEM) and a VGHB5 Vaccuum Generator HB5 Scanning Transmission Electron Microscope (STEM) were used.

Electron energy loss spectroscopy (STEM). Spatial resolution is about 2 nm. Carbon sensitivity is very high (better than 100 atoms). Special precautions were observed to avoid contamination on the alumina carrier alone and on the fresh catalysts.

Electron diffraction, in selected area mode (CTEM) or in microdiffraction mode (STEM) (with spatial resolution varying continuously from 2 nm to 1 μm) (*25*).

3. RESULTS

3.1. Catalytic Consequences of Coke Deposition

For the isomerization/cracking test on the monometallic catalyst (Pt (0.6%)/Cl (1.6%)/Al_2O_3), *n*-heptane conversion as a function of coke content is plotted in Fig. 1. (The coke deposition reaction was carried out between 10 and 90 min to obtain the required coke contents). It can be observed that (1) a large mass of carbon is deposited in the initial operating period, (2) the same amounts of coke deposited after a certain operating time interval have a lesser effect on catalyst activity than if deposited from

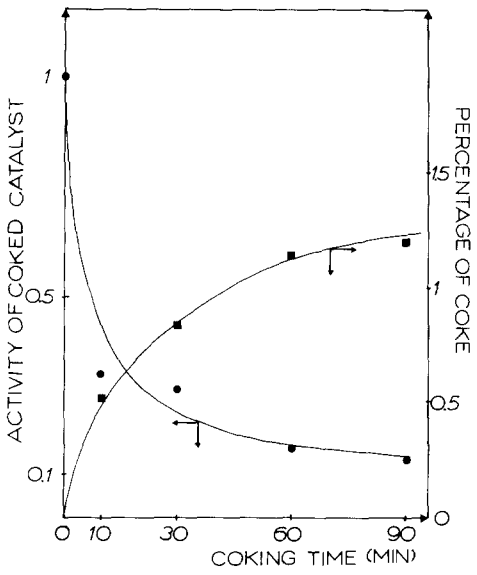

FIG. 1. Variation of catalyst activity and percentage of coke deposited with coking time.

the onset of coking, and (3) selectivity is altered (Fig. 2). Among the products of the isomerization/cracking test, which ranged from methane to heptane and its isomers, we were specifically interested in the families (C_1 + C_2) and (C_3 + C_4) and in the isomers of *n*-heptane. In fact, the pair (C_1 + C_2) is more easily obtained by the monofunctional metallic hydrogenolysis reaction (*26*). By contrast, the hydrocarbons (C_3 + C_4) are obtained preferentially by the hydrocracking reaction involving a bifunctional mechanism (*27*). While selectivity (number of moles of *X* obtained per 100 moles of *n*-heptane input) for (C_1 + C_2) and for (C_3 + C_4) decreases significantly, the isomerization selectivity (2-methylhexane and 3-methylhexane) increases.

The variation in benzene hydrogenation offers an indication of the effect of coke deposition on the metallic function (Fig. 3). A sharp drop in activity is observed for the benzene hydrogenation reaction.

3.2. Analysis of the Macroscopic Distribution of Coke

Following the coking reactions, different colours of the catalyst grains can be observed. Whereas the fresh and reduced catalyst is greyish in colour, visual observation usually shows a very deep and uniform black for the used catalyst. For slightly coked catalysts, however, a darkish brown colour is observed. We therefore decided to observe several catalysts with different coke percentages by optical microscopy.

3.2.1. Observation by Optical Microscopy

Plate 1 shows a comparison of the fresh specimen with two coked catalysts, namely Pt (0.6%)/Cl (1.6%)/Al_2O_3 with coke at 1.5% and 16.5% and coking conditions 1 (Table

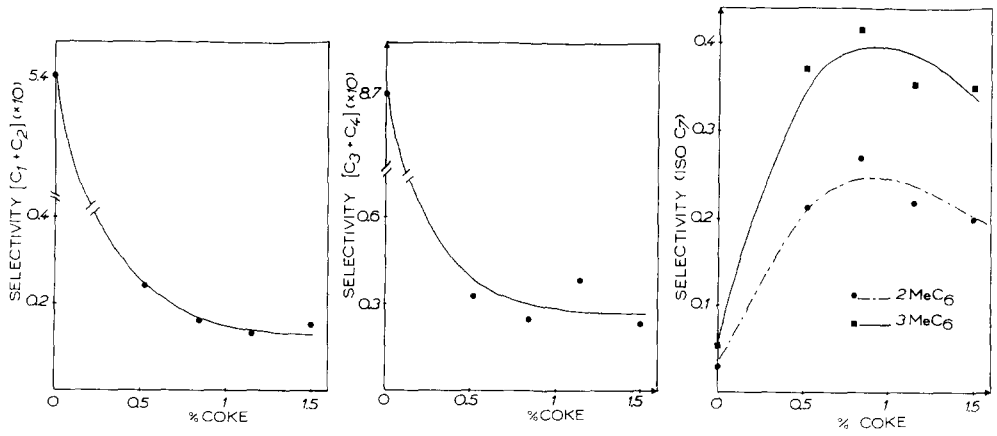

FIG. 2. Variation in catalyst selectivity during coking.

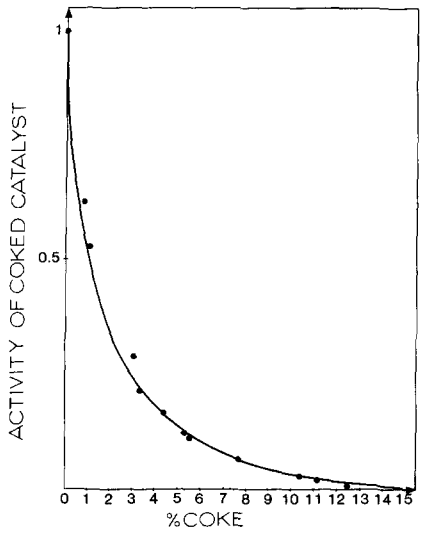

FIG. 3. Variation in catalyst activity for benzene hydrogenation during coking.

2). The fresh catalyst shows whitish crystals of uniform colour. on the slightly coked sample (1.5%) next to the small greyish deposits large black blocks some 50 μm in size now appear; these are never found in the fresh catalyst. As the percentage of coke increases (16.5%), the dark areas increase to produce the darker aspect of the catalyst. The dark zones which increase with the coke percentage are defined as coked regions. The brighter zones correspond to grains that are probably less coked.

3.2.2. Analysis of the Carbon Distribution in the Extrudate by Electron Microprobe

Given the weak response of carbon, we analyzed a monometallic catalyst (Pt (0.61%)/Cl (1.47%) deposited on γ_c-alumina and containing 9.46% coke (coking conditions 1 (Table 2)). The sample analysis is shown in Fig. 4.

An average signal of 2300 counts was obtained on carbon for the coked sample. The background noise is about 260 counts on the corresponding fresh catalyst and in the same conditions. The concentration profile reveals many discontinuities. Two types of region can be distinguished:

(i) Fairly extensive zones (A in Fig. 4) measuring about 60 μm, where the signal detected is higher than the average value observed on the overall extrudate. Large areas are therefore found where the percentage of coke is higher than the average percentage of the deposited coke.

(ii) Smaller zones of about 10–20 μm (B in Fig. 4) producing intense peaks indicating a higher carbon concentration. These peaks imply the presence of large coke deposits (around 10 μm) given the weak response of carbon.

3.2.3. Coke Distribution Observed by Ion Microprobe

We used this instrument to analyze a coked bimetallic catalyst (1.15% coke, coking conditions 1 (Table 2)) based on platinum and iridium (Pt (0.58%)/Ir (0.08%)/Cl (1.51%)). The concentration profiles are shown in Fig. 5.

The aluminum signal shows few disturbances and defines the "roughness" on the extrudate surface. The profiles on platinum, iridium, and chlorine perfectly follow the aluminum signal, indicating a homogeneous distribution of the active elements within the extrudates at least at the scale of the ion

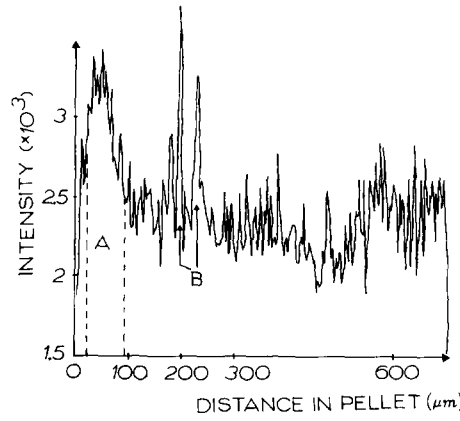

FIG. 4. Concentration profile of coke across the extrudate determined by electron microprobe.

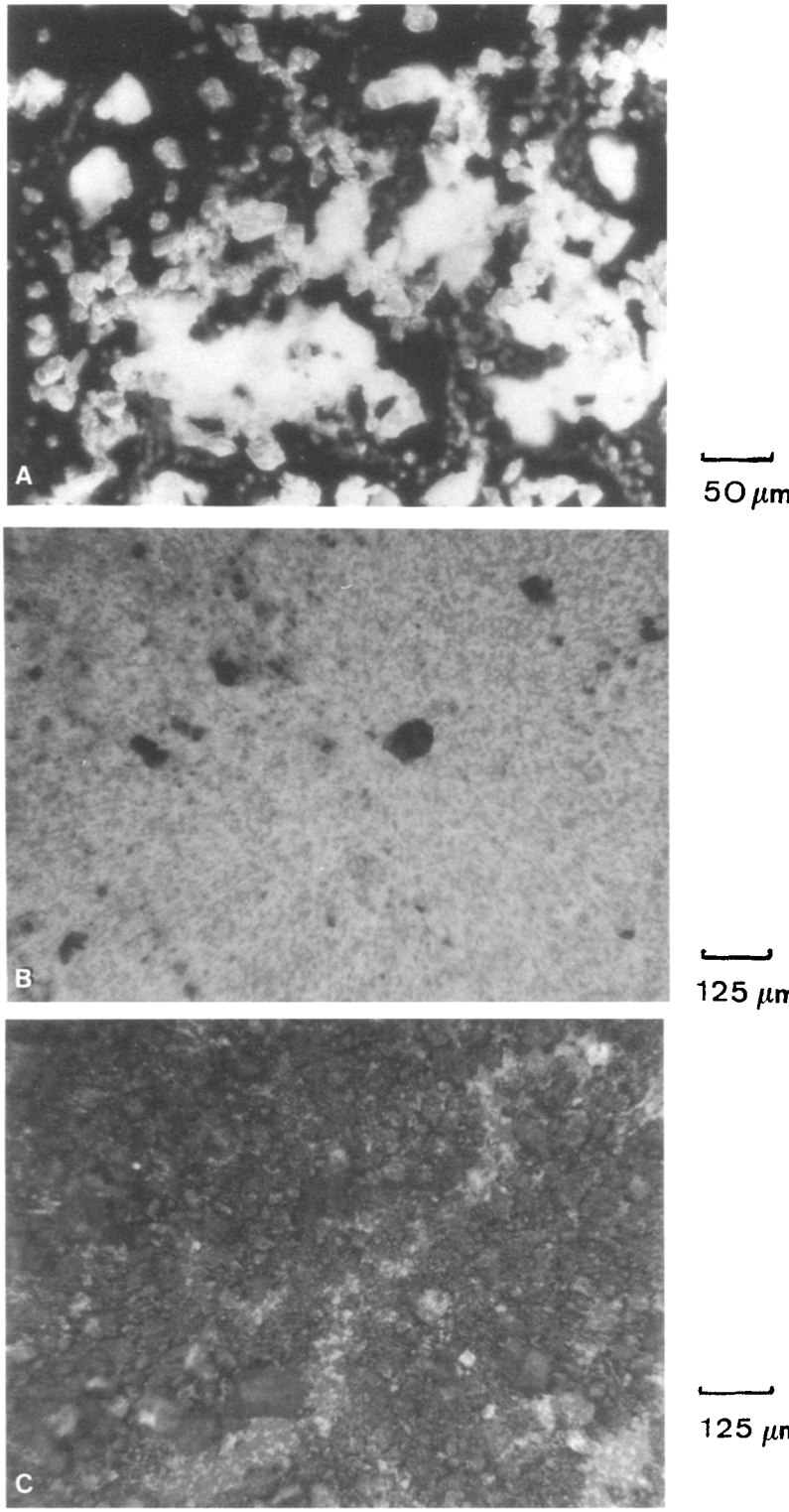

PLATE 1. Views of coked catalysts at different magnifications: (A) Fresh catalyst; (B) 1.5% coke; (C) 16.5% coke.

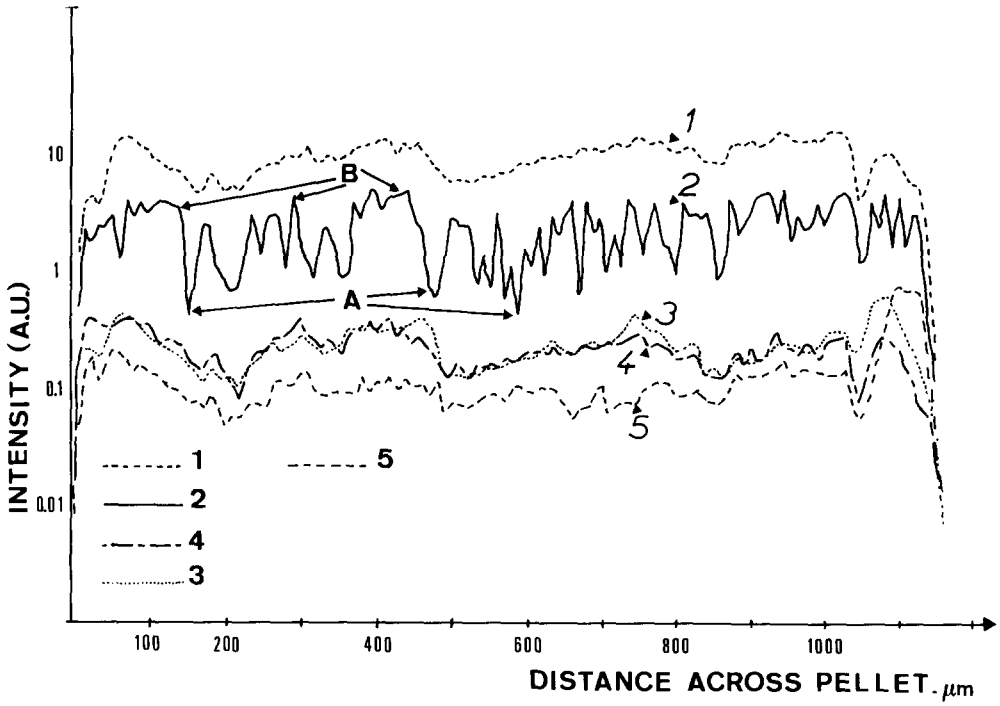

FIG. 5. Distribution profile of coke obtained by ion microprobe: (1) Al; (2) C; (3) Ir; (4) Pt; (5) Cl.

microprobe. For the carbon profile, however, very wide irregularities are observed in the signal intensity, as in the analysis obtained by electron microprobe.

Two different regions can be distinguished, namely areas quite free of coke (zones A) where the carbon signal is very low, and areas (zones B) where, on the contrary, the peak signal, close to the maximum observed, reaches a size of about 20 to 100 μm.

3.2.4. Sorptometry Studies

This study concerned seven monometallic catalysts (Pt (0.55%)) coked to increasing contents (Table 3). The coking conditions were identical for the first six samples A–F but for sample G with a very high coke concentration (27.31%), we used more severe coking conditions. The results obtained on the samples are shown in Table 3. On the whole, the pore volume and specific area can be seen to decrease with increasing percentage of coke. The grain density increases, while the structural density decreases.

Considering the pore volume and surface area as a function of coke percentage (Fig. 6), we can observe a practically linear decrease in the pore volume. Simultaneously, the surface area decreases sharply at low coke contents, and then changes only slightly at a high carbon concentration.

The pore distribution is also strongly affected by coking (Fig. 7). On catalyst G, all the pore sizes are affected by the coke. An increase in the number of pores smaller than 50 Å, resulting from the filling of the larger channels, can also be observed.

An examination of the variation in structural density with coke deposition is interesting, because it serves to calculate the density of the coke deposited. Let us consider the coked catalyst model shown in diagram A in Fig. 8. For 1 cm^3 of catalyst, we have the equations

$$V_{CN} + V_C = 1 \qquad (1)$$

TABLE 3

Definition of Catalysts Investigated and Results of Sorptometry Studies

	Catalyst[a]						
	A[b]	B[b]	C[b]	D[b]	E[b]	F[b]	G[c]
Percentage of coke deposited	0	1.63	3.63	8.52	12.56	22.55	27.31
Total Pore Volume ($cm^3\ g^{-1}$)	0.60	0.62	0.61	0.49	0.52	0.40	0.39
Grain density	1.12	1.02	1.02	1.14	1.21	1.43	1.46
Structural density	3.39	2.67	2.58	2.36	2.68	2.61	2.50
Surface area ($m^2\ g^{-1}$)	203	196	186.5	169	171	180	173
Cylindrical pore model							
Surface area ($m^2\ g^{-1}$)	234	227	214	178	167	188	160
Volume ($cm^3\ g^{-1}$)	0.64	0.61	0.61	0.54	0.52	0.44	0.39
Slit pore model							
Surface area ($m^2\ g^{-1}$)	194	187	176	150	146	146	125
Volume ($cm^3\ g^{-1}$)	0.64	0.60	0.60	0.54	0.52	0.43	0.40

[a] Pt (0.55%)/γ_c–Al_2O_3.
[b] Coking conditions. Temperature: 803 K, PPH (defined in Table 2): 3.5, H_2/HC: 1, P: 5 bar, feed injected: nC_7.
[c] Coking conditions. Temperature: 803 K, PPH (C_6H_6): 0.5, H_2/C_6H_6: 1.6, P: 5 bar, feed injected: $nC_7 + C_6H_6$.

$$M_{CN} + M_C = d_{sc} \cdot \rho_0 \quad (2)$$

($\rho_0 = 1\ g\ cm^{-3}$)

$$\frac{M_{CN}}{V_{CN}} = d_{sn} \cdot \rho_0 \quad (3)$$

$$\frac{M_C}{M_{CN}} = \frac{\tau}{100} = \tau' \quad (4)$$

where

V_{CN}: volume of fresh catalyst
V_C: volume of coke
M_{CN}: mass of fresh catalyst
M_C: mass of coke
d_{sc}: structural density of coked catalyst
d_{sn}: structural density of fresh catalyst
τ: percentage of coke.

We obtain the coke density $\rho_c = M_C/V_C$ given by the formula

$$\frac{1}{\rho_c} = \frac{\tau' + 1}{\tau' d_{sc} \rho_0} - \frac{1}{\tau' d_{sn} \rho_0} \quad (5)$$

The results obtained by application of this formula to catalysts B–G are shown in Table 4. For low coke contents, the value of ρ_c is especially low. As the coke content rises, ρ_c increases. This variation cannot be explained by a structural change of the coke during coking, especially in the light of the density values for certain carbonaceous products such as benzene (density 0.87), anthracene (density 1.28), and graphite (density 2.26).

The only possible explanation is pore plugging without filling. Consider the coked catalyst model in diagram B of Fig. 8. In

TABLE 4

Coke Density Calculated for Different Coked Catalysts

Percentage of coke	d_{sc}	ρ_c ($g\ cm^{-3}$)
1.63	2.67	0.19
3.63	2.58	0.34
8.52	2.36	0.52
12.56	2.68	1
22.55	2.61	1.29
27.31	2.50	1.27

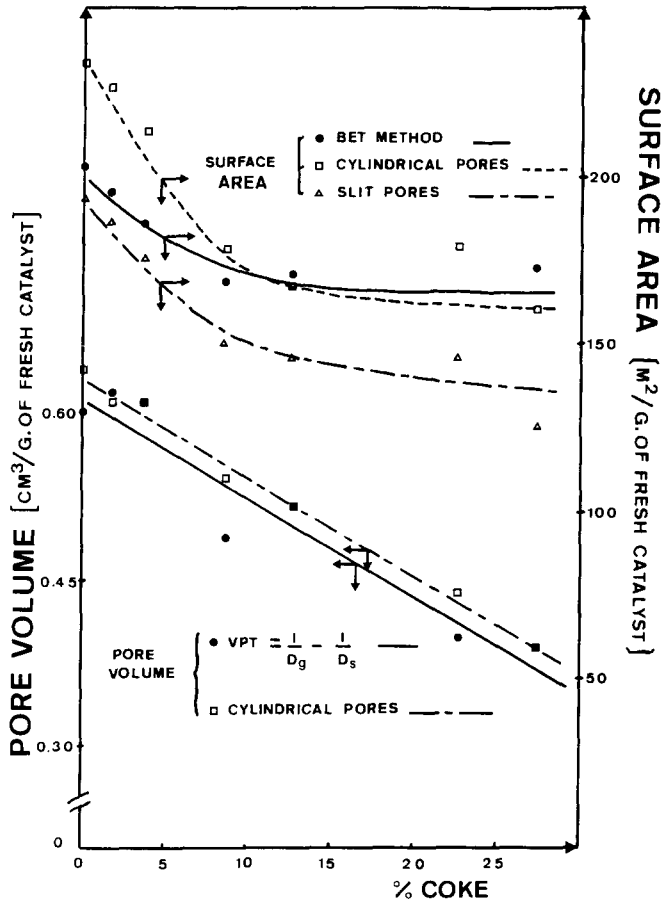

FIG. 6. Variation in pore volume and surface area as a function of coke percentage.

comparison with the foregoing equations, it is necessary to consider the void pore volume V_V isolated from the rest of the catalyst. The new equations are therefore

$$V_{CN} + V_C + V_V = 1 \qquad (1')$$

$$M_{CN} + M_C = d_{sc} \cdot \rho_0 \qquad (2')$$

($\rho_0 = 1$ g cm^{-3})

$$\frac{M_{CN}}{V_{CN}} = d_{sn} \cdot \rho_0 \qquad (3')$$

$$\frac{M_C}{M_{CN}} = \frac{\tau}{100} = \tau'. \qquad (4')$$

The expression for ρ_c thus becomes

$$\frac{1}{\rho_c} = \frac{\tau' + 1}{\tau' d_{sc} \rho_0} - \frac{1}{\tau' d_{sn} \rho_0} - \frac{V_V}{M_C}. \qquad (5')$$

This expression again shows the terms of Eq. (5), but with a corrective term added equal to V_V/M_C. If the isolated volume V_V is determined from the first coke percentages, and remains constant, the increase in deposited coke (M_C) tends to diminish the effect of the factor V_V/M_C. Thus the apparent density of the coke given by Eq. (5) approaches the true density of the coke as the carbon content increases (Table 4).

3.3. Localization of Coke on a Microscopic Scale

Two types of techniques were used, namely conventional transmission electron microscopy and electron energy loss spectroscopy.

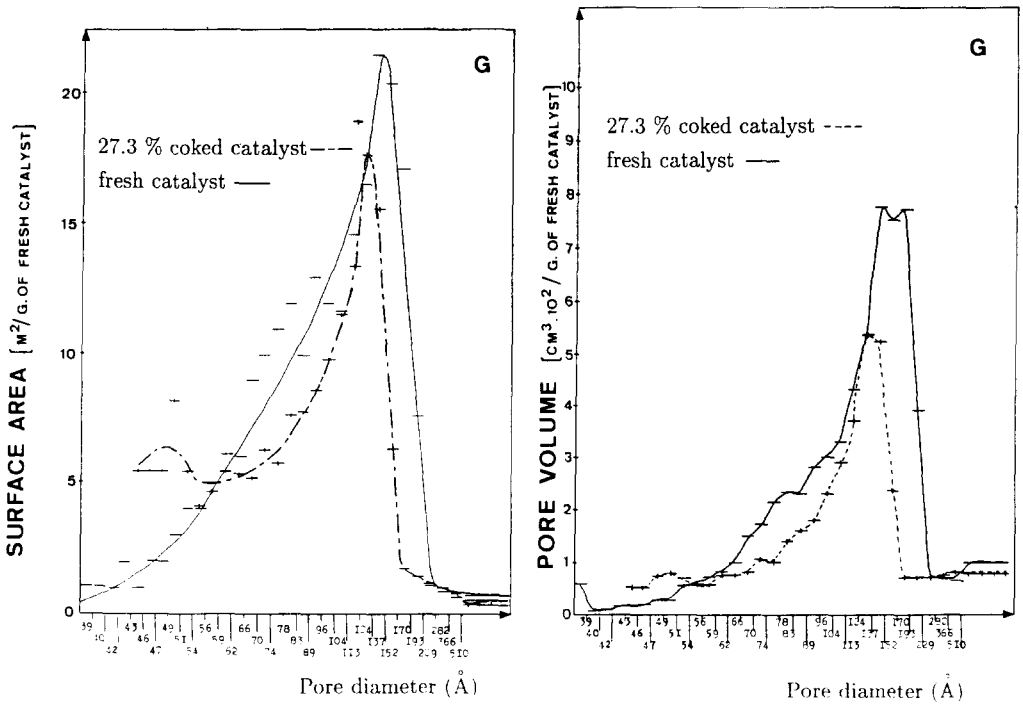

FIG. 7. Pore distribution curves.

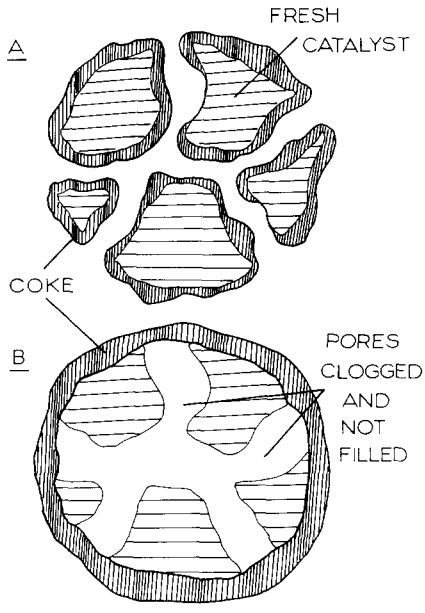

FIG. 8. Coke localization model.

3.3.1. Conventional High-Resolution Microscopy

We successively examined the fresh catalyst and the coked catalyst containing 27.3% coke (sample G, Table 3).

Plate 2 gives a general view of the fresh catalyst. The support consists mainly of plate-like particles 30 to 50 nm long, 5 to 10 nm wide, and 3 to 5 nm thick. These particles are gathered together in noncomposite clusters, making up the catalyst micrograins. With an inclined beam and at high resolution, the crystallographic planes (222) and (400) (d = 0.228 and 0.198 nm respectively) of the alumina are revealed (Plate 3). For the coked catalyst (Plate 4), three types of zone can be distinguished.

In a coke-free zone (Plate 4, Zone A) the sample is identical in all respects to the fresh catalyst. Any coke present in these zones must be in the form of a very thin layer.

Slightly-coked zones (Plate 4, Zone B)

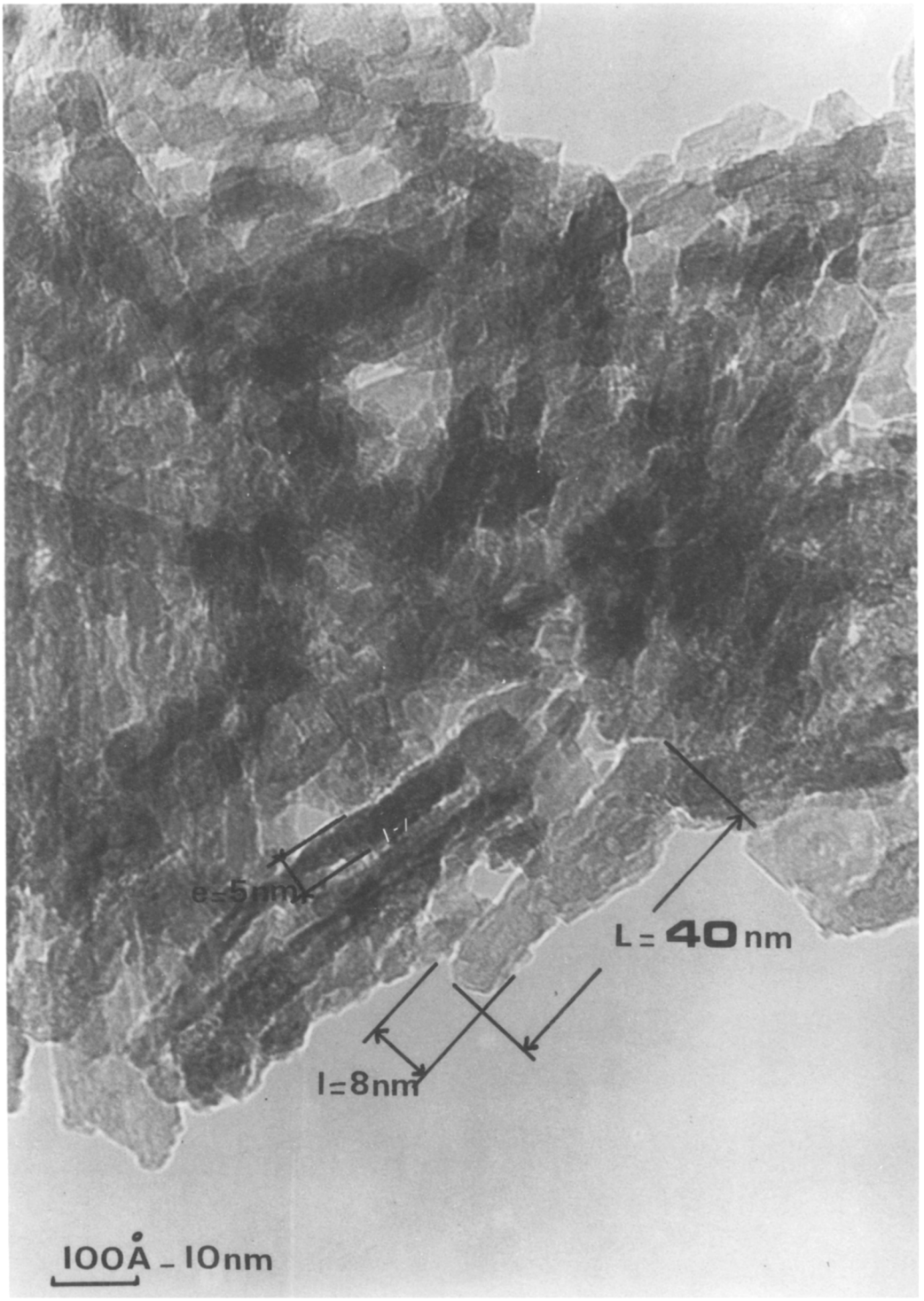

PLATE 2. General view of fresh catalyst by conventional transmission electron microscopy (CTEM).

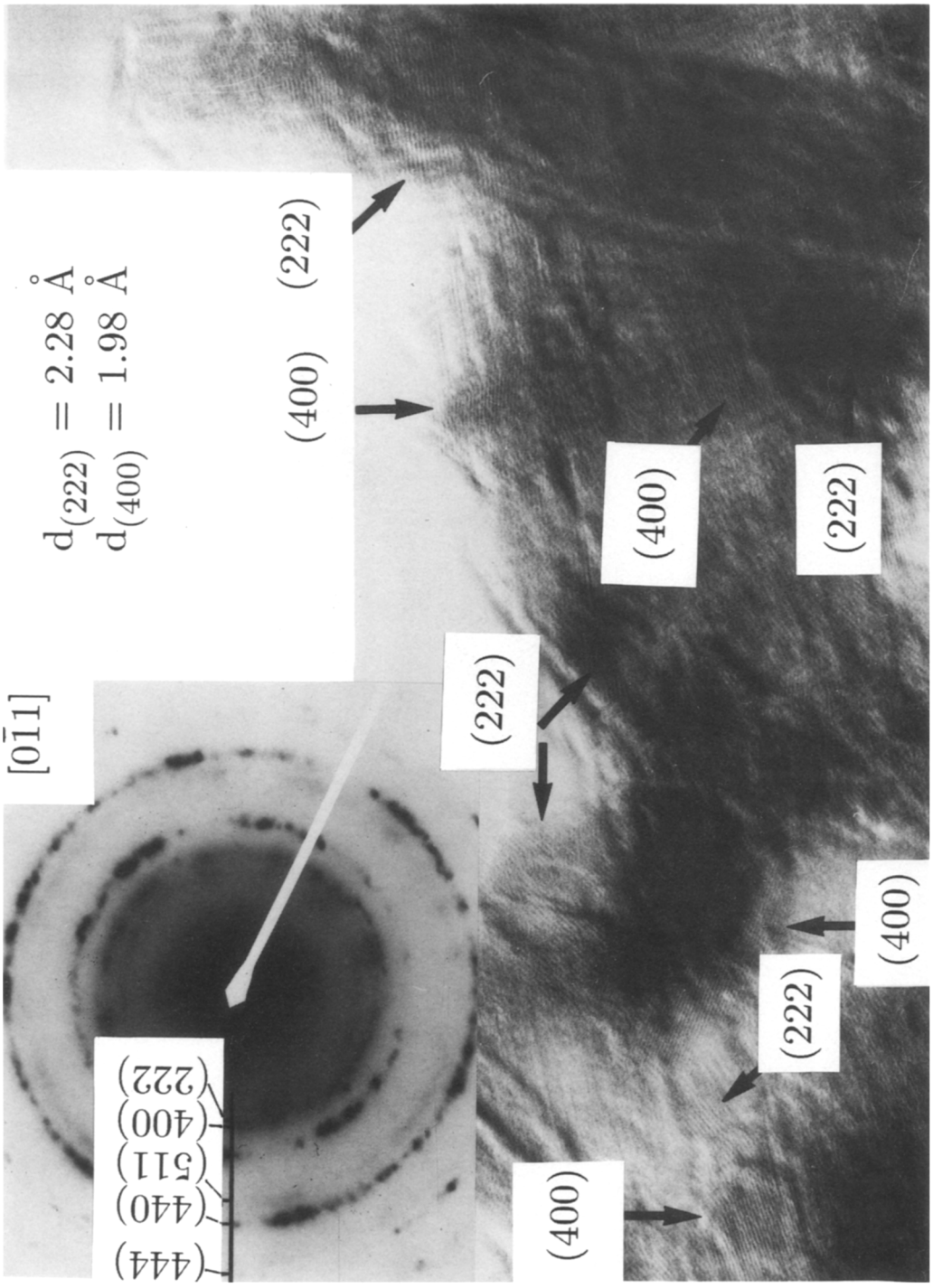

PLATE 3. Crystallographic planes (222) and (400) of alumina on catalyst.

PLATE 4. View of coked catalyst by electron microscope.

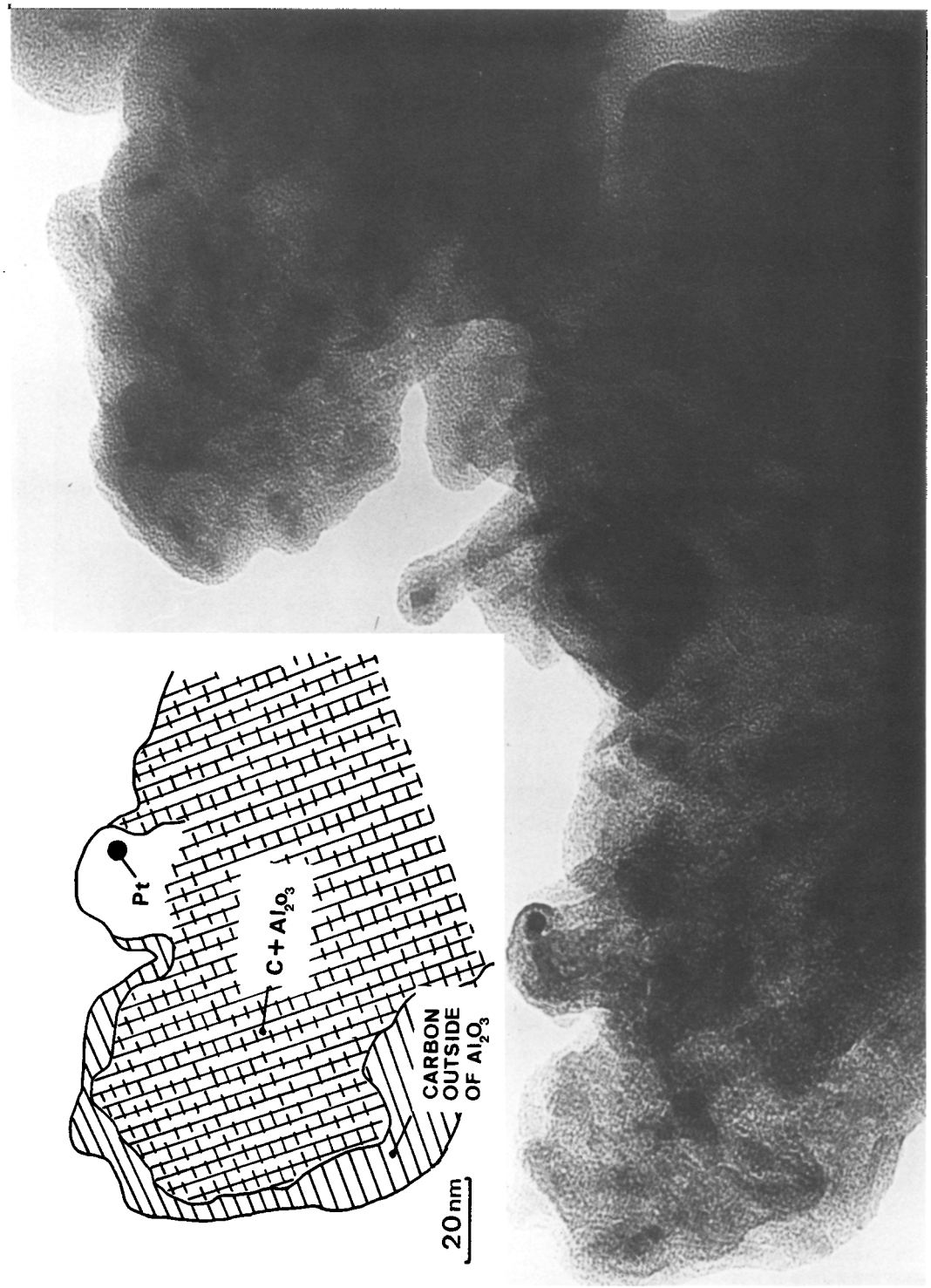

PLATE 5. Highly coked zone viewed by conventional electron microscopy.

clearly highlight a layer of pregraphitic carbon. This layer only exists in places and the carbon is generally poorly organized. The coherent regions only measure a few Å, and the crystallographic (002) distances appear to be greater than those of graphite (0.35 to 0.37 nm against 0.335 nm for graphite). The fact that this carbon can be visualized implies a thickness of few atomic layers. Certain zones reveal a much better organized carbon. These zones are identified by black arrows in Plate 4. Despite the nonrectilinear projections, the crystallographic planes (corresponding to graphitic sheets) extend over about 15 Å and offer a characteristic image of a small crystallite. These lamellae in the process of organization may grow three-dimensionally, and the coke could thus completely cover the support (Plate 4, Zone C).

In highly coked zones, the support is buried in the coke (Plate 5) which is up to several hundred Å thick. Here also the coke is poorly organized or amorphous. Note in addition the presence of a platinum crystallite, with the metal imperfectly dispersed. The metal appears to be covered with coke and fairly well organized structures can also be seen in its vicinity.

3.3.2. Analysis of a Coked Catalyst by Electron Energy Loss Spectroscopy

The sample was identical to that in Sec. 3.3.1. Several zones measuring about 5 nm

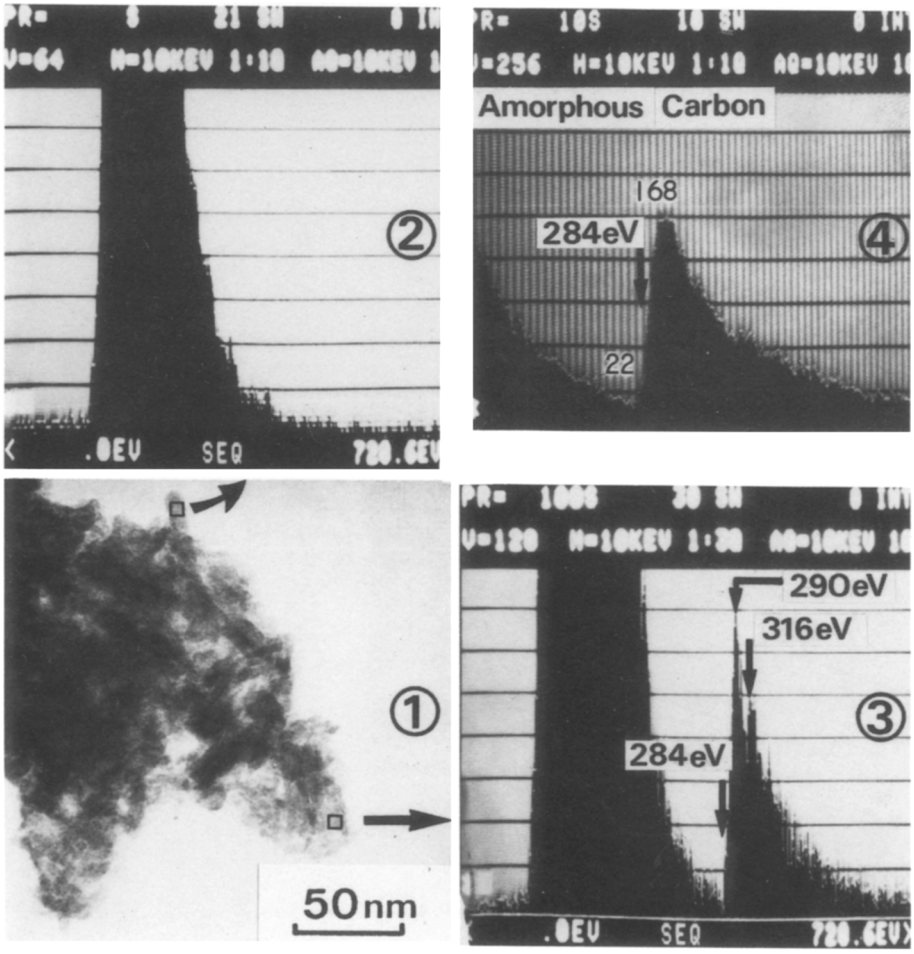

PLATE 6. Analysis of a coked catalyst by electron energy loss spectroscopy (EELS).

were analyzed by electron energy loss spectroscopy (Plate 6). For zone 2, with a very similar aspect of the previous A-region (Plate 4), the energy loss spectrum shows only two peaks, the elastic peak and the plasmon peak. By contrast, zone 3, identical to zones B or C (Plate 4), clearly shows the K edge of the carbon (284 eV) and the clearly-defined EXELFS oscillations. The comparison of this spectrum with the one obtained on an amorphous carbon (Plate 6) clearly shows a specific EXELFS structure, mainly displaying two more intense peaks at 290 and 316 eV. These observations confirm the local existence of a rather well organized carbonaceous deposit.

3.4. Analysis of the Coke Structure

The analysis of the coke localization revealed the existence of carbonaceous deposits of varying thickness on the catalyst, in a large size range from a few dozen microns to a few Å. Electron microscopy showed that the coke could be organized to some extent. We shall now clarify this point by directly analyzing the used catalyst or the coke after dissolution of the catalyst support.

3.4.1. X-Ray Diffraction Analysis

3.4.1.1. Analysis of coked catalyst. The diffraction patterns of three specimens (Pt (0.55%)/γ_c-Al_2O_3), S1, S2, and S3, with increasing coke percentages are shown in Fig. 9. Sample S1 is the fresh catalyst, and catalysts S2 and S3 have coke contents of 11.5 and 27.3% respectively. Sample S3 is very similar to specimen G (Table 3); S2 was coked following coking conditions 1 (Table 2). The overall diffractogram shows an increase in the signal due to carbon scattered intensity. This is especially intense at the low angles. A characteristic band at about 2θ = 25 degrees (d = 3.56 Å distinguishes the spectra of the coked catalysts from that of the fresh catalyst. It corresponds to the line (002) of pregraphitic carbon ($d_{(002)}$ = 3.35 Å). This measurement confirms the degree of organization of the coke that was identified by electron energy loss spectros-

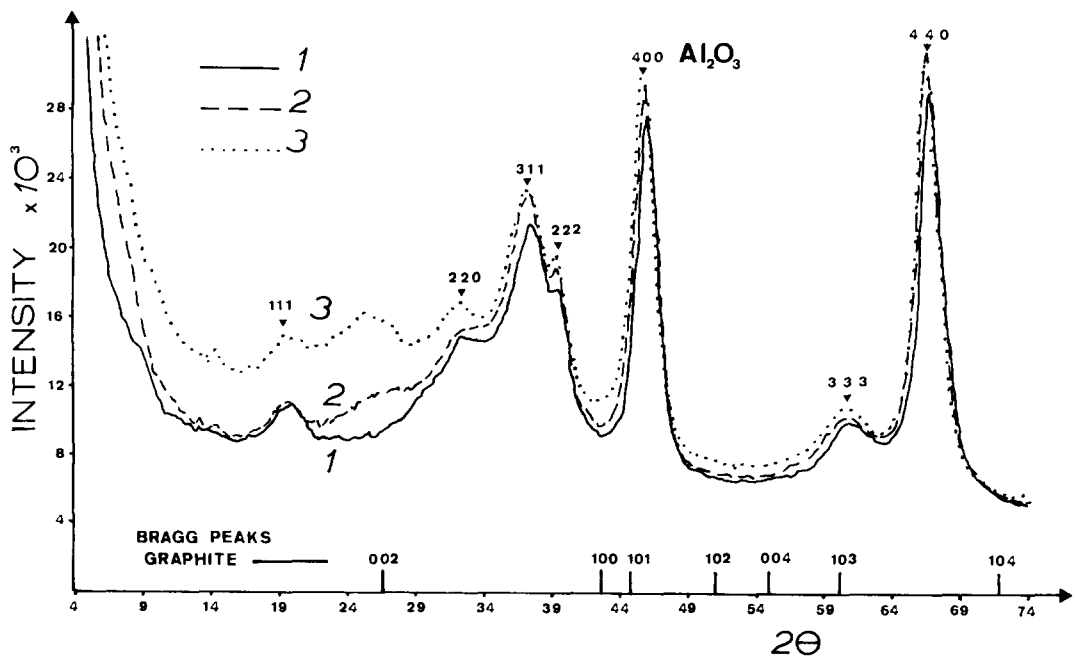

FIG. 9. X-ray diffraction spectra of coked catalysts: (1) S1 (fresh catalyst); (2) S2 (11.5% coke); (3) S3 (27.3% coke).

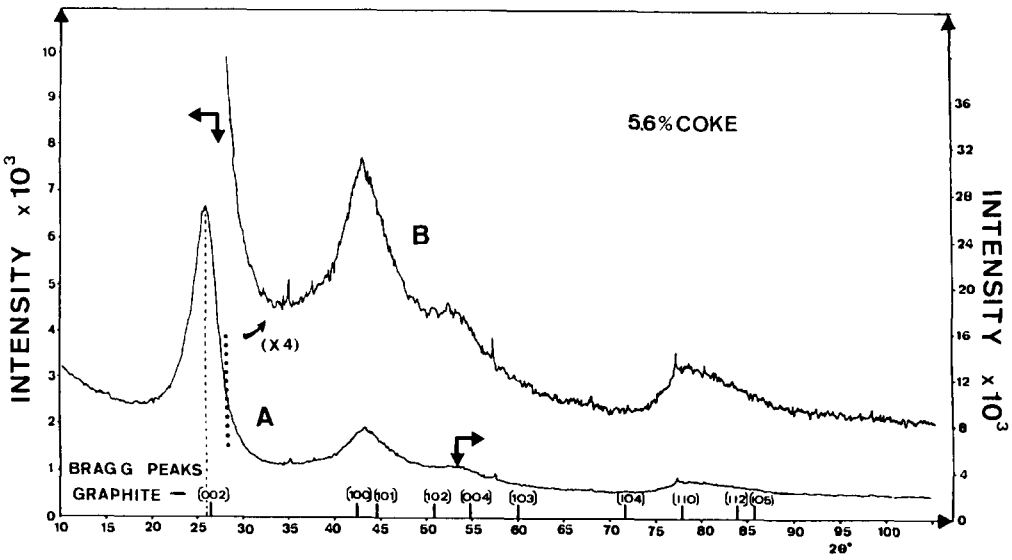

FIG. 10. X-ray diffraction patterns of coke. The two curves (A, B) correspond to different scale intensities.

copy. In the diffraction spectra (Fig. 9), however, the carbon signal remains very weak even at high coke ratios, and is often masked by the signal of alumina.

3.4.1.2. Analysis of residual coke after acid attack. For this study, we considered a catalyst (Pt (0.55%)/Al_2O_3/coking conditions 1 (Table 2)) containing 5.6% coke, from which the alumina support was removed by acid attack (Section 2.4).

The diffraction pattern obtained is shown in Fig. 10. Note first an intense diffraction band corresponding to line (002) well-known in carbonaceous compounds, and representing the stacking of the graphite sheets. We succeeded in determining the spacing between these sheets, which measured 3.5 Å. Using the Scherrer equation ($L_{002} = \lambda/\Delta\theta \cos\theta$) we calculated the size of the crystalline regions (002) to be close to 30 Å, corresponding to about ten superimposed sheets.

On an expanded scale (B), it is possible to distinguish other lines. By referring to the positions of the Bragg peaks of graphite (Fig. 10) one can observe that the diffraction spectrum of the coke is quite similar to that given by graphite. Apart from the band corresponding to line (002), the most intense band lies at $2\theta = 43.25$ degrees, or $d = 2.09$ Å. This corresponds to the sum of the two bands corresponding to (100) and (101). We thus verified a crystallographic organization of the particle along these two directions ((100) and (101)).

3.4.2. Local Characterization of Coke by High-Resolution Imaging and Electron Diffraction

The carbon residue from acid attack of the previous catalyst used for X-ray diffraction study was observed.

3.4.2.1. Electron diffraction on selected area of coke. Several crystals resulting from acid attack were deposited on the sample grid and analyzed by electron diffraction of a selected area. The different situations encountered are summarized by the four diagrams in Plate 7.

The first, A, shows three diffuse rings corresponding to the graphite planes (002), (100), and (110). They closely reflect a powder diagram, but with a preferential orientation corresponding to the spotting of the two

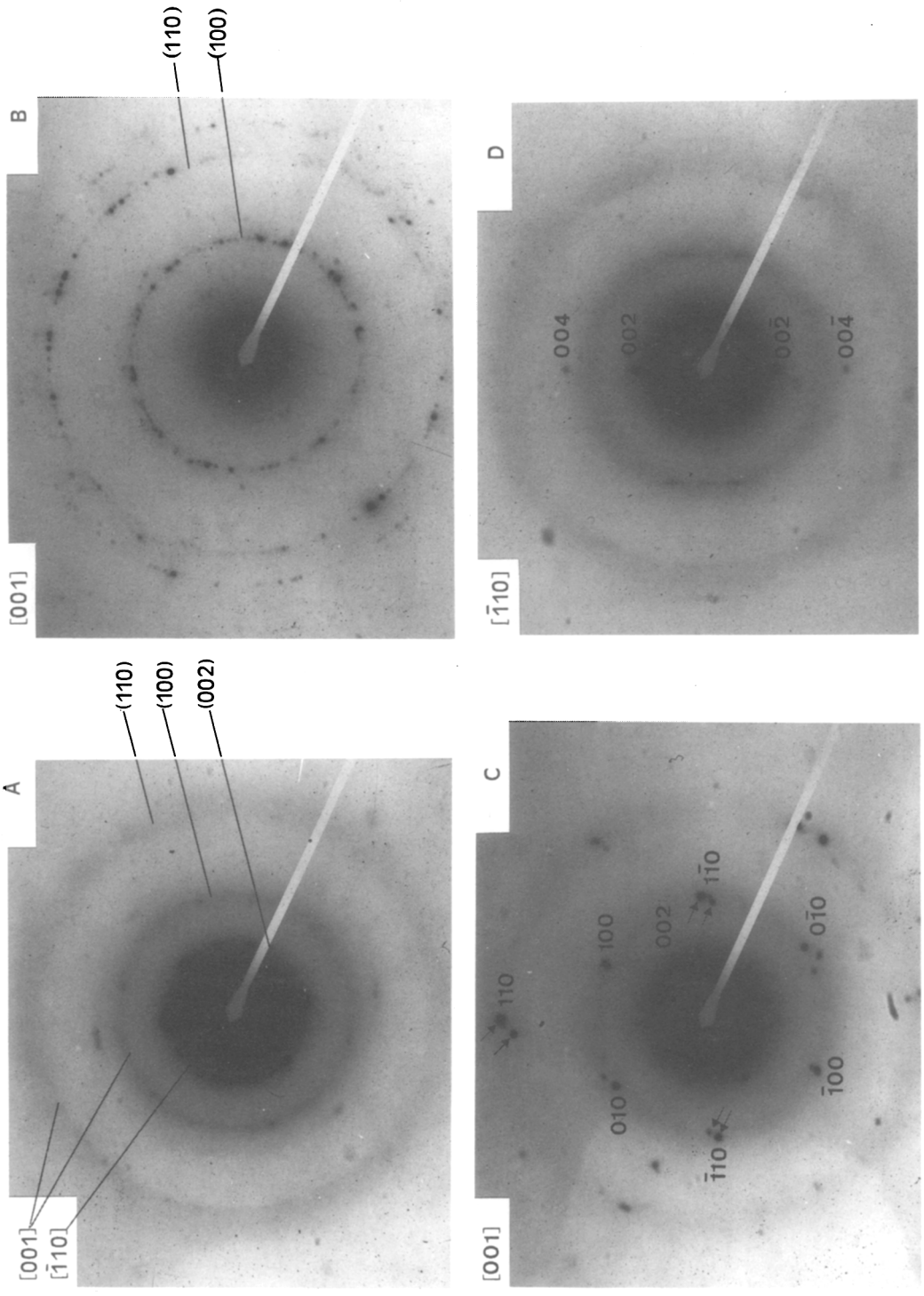

PLATE 7. Electron diffraction in selected area on coke after dissolution of alumina carrier.

rings (002) and (100). The zone analyzed is hence formed of many monocrystals.

The second diagram, B, reveals a preferential growth in the graphitic plane. The change from diagram A is clearly visible. The rings (100) and (110) are spotted and ring (002) simultaneously disappears. Moreover, note that ring (100) is no longer perfectly circular, but becomes elliptical. This reflects the existence of a turbostratic carbon. The graphitic planes exhibit a slight mutual rotation about axis 001.

Diagram C is formed of points located on a hexagon, indicating the hexagonal structure of graphite. The region analyzed is therefore probably well crystallized. A doubling of the diffraction spots (see arrows) is also observed, recalling twinning. Also visible are the spots (002) for which axis 001 is not the zone axis. This may reflect an ordered coke growth.

Case D shows two very intense spots (002). Contrary to case B above, the stacking of sheets is faster than the growth in the plane.

All these results show a certain heterogeneity of the structure of the coke deposited on the catalyst. To clarify all these data, it was decided to produce an even more local image of the coke structure using electron microdiffraction.

3.4.2.2. Coke analyzed by electron microdiffraction. Plate 8 shows the analysis conducted on six distinct zones of a coke deposit collected after acid attack.

The first three pictures show the two rings (100) and (110). In the first diagram, however, both rings appear circular, whereas in the second, third, and fourth, the rings become elliptical. This reveals an inclination of the zone analyzed in relation to the incident electron beam. In the reciprocal space, given the small sample sizes, we have cylinders whose axis is parallel to the electron beam. If the sample is inclined, the intersection of the diffraction plane with the cylinder gives ellipses. This can be observed with increasing inclination in pictures 2, 3, and 4. However, we can see that pictures 1, 2, and 3 are spotted, indicating an imperfect organization of the planes, and confirming the turbostratic character of the carbon deposited. This does not apply to pictures 4, 5, and 6, in which the order appears more clearly. Picture 4 shows the carbon planes, and planes (001) appear in pictures 5 and 6. In the latter case, the three-dimensional order is visible simultaneously with a good organization in the planes.

3.4.2.3. High-resolution images of coke after dissolution. A number of interesting views of the coke obtained by conventional electron microscopy (Plate 9), showing probably the largest deposits on the catalysts, were selected. The first photograph shows a carbonaceous deposit which certainly matched the shape of the pore, whose traces can be identified. Some 20 planes (002) were counted. The alumina has disappeared during dissolution, leaving these sheets as a remainder from the volume that they occupied.

The second picture also shows fairly rectilinear planes. Each deposit has some 15 graphitic planes, which agrees with the X-ray diffraction results.

4. DISCUSSION

The results of the catalytic tests clearly show that all the metallic and acidic functions are affected by coking. A pronounced loss of activity also occurs from the onset of coking. This clearly demonstrates the importance of catalyst conditioning, during which the catalyst activity is reduced. This loss of activity is not identical for the different reactions occurring during reforming, resulting in a change in selectivity. The sites capable of promoting the cracking of the molecules are more affected than those responsible for isomerization. For the metallic function, the hydrogenolysing sites are more poisoned than the benzene hydrogenating sites.

Great heterogeneity also appears in the coke distribution on the catalyst. As to the coke distribution and texture, two essential points stand out. The coke is not dispersed

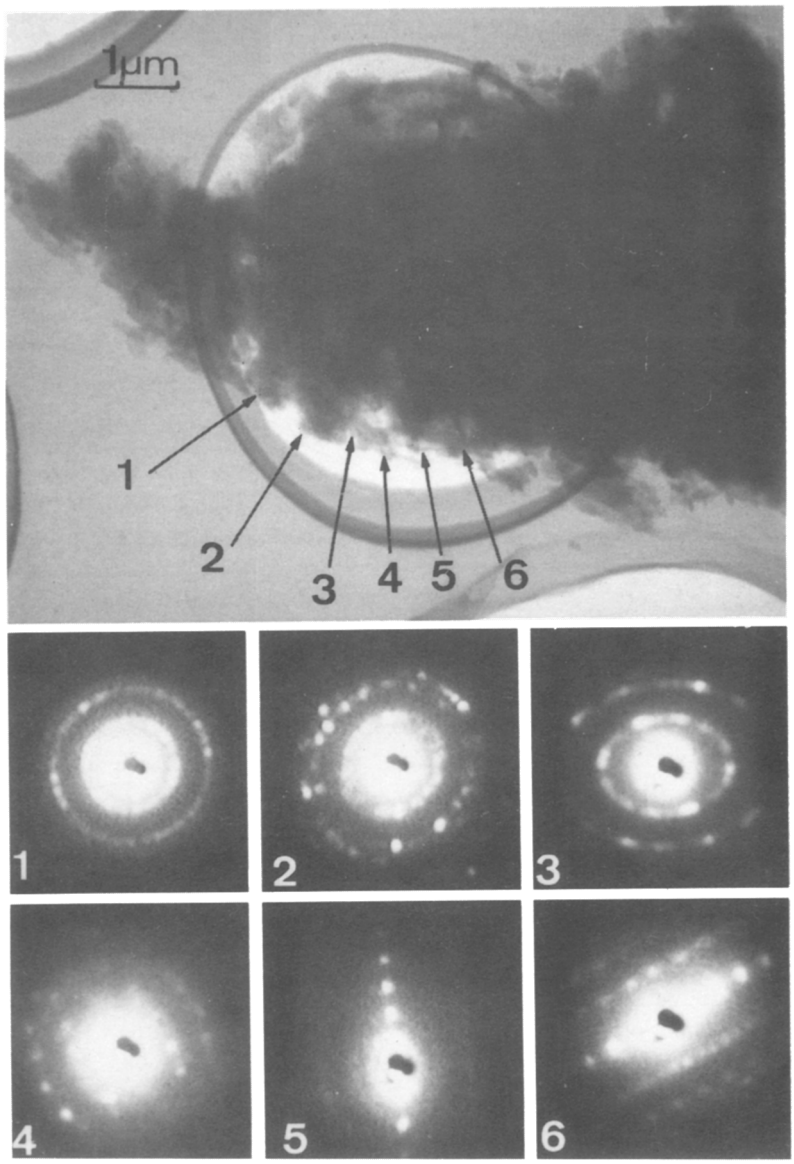

PLATE 8. Examples of coke microdiffraction after dissolution of alumina carrier.

in the form of a monolayer. On the contrary, three-dimensional deposits appear from the onset of coking. The highly heterogeneous character of the deposit on the scale of 1 μm, as demonstrated by electron and ion microprobes, extends to the scale of 1 nm. The same applies on the microscopic scale. On a very highly coked catalyst, it was possible to identify simultaneously zones buried in coke and, by contrast, zones that were only slightly coked, if at all. Referring to the Raman spectroscopy study (*13*) which is more sensitive to the carbon content, it appears that the coke deposits covering the catalyst surface heterogeneously are present at the beginning of coking. The deposits which grow locally may plug the pores and prevent molecules from reaching part of the

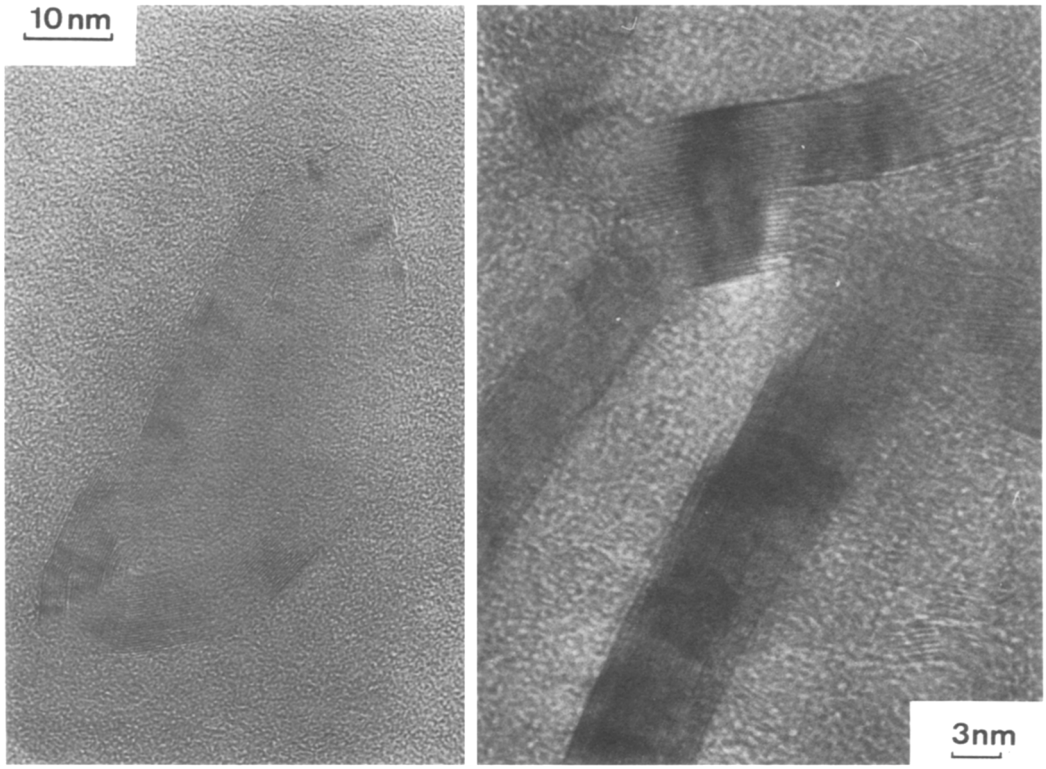

PLATE 9. Conventional high-resolution microscopic view of coke after dissolution of alumina carrier.

catalyst. Two hypotheses can be considered to explain this heterogeneity of coke deposition.

The first is that the heterogeneous deposits depend on a specific local activity. It has been pointed out that, if the support has some macroporosity, the catalyst is more stable (unpublished results from Institut Français du Pétrole and patents). Another possibility is a structural heterogeneity of the alumina support. Observation of alumina supports for catalysts shows that they are generally microcrystalline. Thus the exposed faces may be different (*28*) and correspond to very different activities that are more or less favorable to coking. Apart from this inherent activity of the alumina, it is also possible that a heterogeneous distribution of the metallic phase and of the chlorine added during impregnation occurs. Note, however, that based on the distribution curves of the metallic elements, chlorine, and carbon obtained by the ion microprobe, no wide heterogeneity appeared on the macroscopic scale. From this standpoint, a more detailed analysis of the elemental composition and a structural analysis would help to identify any differences between coked and uncoked regions.

The second hypothesis is that coke deposition results exclusively from a random process, in which the coke precursors grow in the gas phase, as postulated by Trimm (*29*) and Bortkevich *et al.* (*5*). They explain the formation of these 'tars' by means of Diels–Alder type reactions involving unsaturated hydrocarbons (olefins). The growth of the coke in this case is a process of nucleation, a process governed essentially by the structure of the solid.

From the structural standpoint, the coke exhibits a high degree of organization, since

TABLE 5

Analysis of Polyaromatics in Reformates

Polyaromatics	Fresh catalyst (ppm)	Coked catalyst (ppm)
α Me-naphthalene	1582	500
β Me-naphthalene	910	382
Higher aromatics up to anthracene	7700	4200
Fluoranthene	13.4	<1
Benzo(a)pyrene	23.8	10.5
Benzo(b)fluoranthene	14.9	1.1
Benzo(ghi)perylene	30	11.3

X-ray diffraction revealed bands identical to those observed for a graphite. A certain heterogeneity of size and structure is identified in electron microscopy. Next to the large deposits whose (001) planes are clearly visible in conventional microscopy, a turbostratic carbon is detected by microdiffraction. In diffraction mode on a selected area, preferential growths in the plane or along the (001) axis were found. Raman spectroscopy (*13*) confirmed the pregraphitization of coke on the catalysts investigated. Starting with paraffinic compounds, a pregraphitic carbon is thus obtained. However, an intermediate step exists for the cyclization, which corresponds to the formation of polyaromatic compounds. We thus succeeded in identifying different polyaromatic species present in reformate and products (Table 5). Note that the quantity of polyaromatics decreases sharply after coking. It can be reasonably assumed that a large part of these species remains adsorbed on the catalyst as poisons. These poisons can probably be desorbed since they are present in the end product, unlike the pregraphitic deposits that are irreversibly adsorbed. The structure of the coke may depend on certain parameters, such as the metallic function or the value of the H_2/HC (*13*). In particular, the increase in the hydrogen pressure, (H_2/HC) ratio on a monometallic (Pt/Al_2O_3) catalyst, gives a Raman spectrum (*13*) that is quite similar to the one obtained on the Pt–Ir bimetallic catalyst. Thus the addition of the second metal would have the same effect as an increase in the hydrogen pressure, and hence a decrease in coke precursors, as was previously postulated by Burch and Mitchell (*30*) and by Coughlin *et al.* (*31*).

Based on the different observations made on coke localization and structure, it can be asserted that coke probably obeys a nucleation mechanism. Seeds and unsaturated molecules are developed in certain regions, which then grow to produce the coke deposits observed. According to the well-known mechanisms of nucleation and growth, a smaller number of initial precursors favors growth in the direction of larger deposits. By contrast, if the catalyst first produces a large number of precursors, the nucleation rate is greater than the growth rate, giving small scattered coke deposits. While it is clear that an increase in the hydrogen pressure generally decreases the quantity of the more or less unsaturated species which are the coke precursors, the question arises as to whether the addition of a second metal can also eliminate all the precursors or only some of them selectively, i.e., those which are very harmful for coking. For instance, some authors (*3, 4, 6*) have shown that certain hydrocarbons are more coking than others, while all of them have stressed the harmful influence of pentane hydrocarbons.

5. CONCLUSIONS

We have demonstrated that the effect of coking varies according to the catalytic reactions carried out, and that metallic or acidic sites are affected differently according to the type of reaction promoted.

The coke localization is very heterogeneous. Certain regions are covered by the carbonaceous deposit, while others remain uncovered. This is true both from the macroscopic and microscopic standpoints. For a better understanding of these differences, it would be interesting to use electron microscopy to characterize the underlying alumina support, both from the structural

standpoint and from the standpoint of the species present at the surface, such as the metallic phase or the chlorine.

Structural heterogeneities of the carbon were also identified. This appears to be well organized, and its structure is strongly influenced by the H_2/HC ratio.

Simultaneously, the effect of certain bimetallic pairs, such as Pt–Ir and Pt–Re, closely resembles that of hydrogen. It would be highly interesting to determine, as suggested during the discussion, whether this actually reflects a change in the production of coke precursors. A fixed analysis of the reaction products, and especially of the polyaromatic compounds, should help to clarify this matter.

REFERENCES

1. Le Page, J. F., "Catalyse de Contact," Technip, Paris, 1978.
2. Bournonville, J. P., and Martino, G., "Proc. Int. Symp. on Catalyst Deactivation, Antwerp, 1980" (B. Delmon and G. F. Froment, Eds.), p. 159, Elsevier, Amsterdam, 1980.
3. Myers, G. G., Lang, N. H., and Weisz, P. B., *Ind. Eng. Chem.* **53,** 299 (1961).
4. Zhorov, Y. M., Panchenkov, G. M., and Kartashev, Y. N., *Kinet. Katal.* **21,** 776 (1980).
5. Bortkevich, M. I., Levinter, M. E., Zabotin, L. I., and Berkovich, L. M., *Kinet. Katal.* **16,** 221 (1975).
6. Cooper, B. J., and Trimm, D. L., "Proc. Int. Symp. on Catalyst Deactivation, Antwerp, 1980" (B. Delmon and G. F. Froment, Eds.), p. 63, Elsevier, Amsterdam, 1980.
7. Barbier, J., Marecot, P., Martin, N., Elassal, L., and Maurel, R., "Proc. Int. Symp. on Catalyst Deactivation, Antwerp, 1980" (B. Delmon and G. F. Froment, Eds.), p. 53, Elsevier, Amsterdam, 1980.
8. Figoli, N. S., *in* "Coke Formation on Metal Surfaces" (L. F. Albright and R. T. K. Baker, Eds.), A.C.S. Symposium Series No. 202, p. 239, 1982.
9. Figoli, N. S., Beltranini, J.N., Martinelli, E. E., Sad, M. R., and Parera, J. M., *Appl. Catal.* **5,** 19 (1983).
10. Parera, J. M., Figoli, N. S., Traffano, E. M., Beltranini, J. N., and Martinelli, E. E., *Appl. Catal.* **5,** 33 (1983).
11. Bakulin, R. A., Levinter, M. E., Galiaxbarov, M. F., Degtjarev, G. S., and Makhonin, G. M., *Khim. Tverd. Topl.* **4,** 82 (1974).
12. Massai, M., Shimadzu, S., Sashiwa, T., Sawa, S., and Minura, M., "Proc. Int. Symp. on Catalyst Deactivation, Antwerp, 1980" (B. Delmon and G. F. Froment, Eds.), p. 261, Elsevier, Amsterdam, 1980.
13. Espinat, D., Dexpert, H., Freund, E., Martino, G., Couzi, M., Lespade, P., and Cruege, F., *Appl. Catal.* **16,** 343 (1985).
14. Sanders, J. V., Spink, J. A., and Pollack, S. S., *Appl. Catal.* **5,** 65 (1983).
15. Standard Oil Company, US Patent 2.848.377, 1953.
16. French Patent 2.372.883, 1976; To Procatalyse 2.373.602, 1976.
17. UOP, US Patent 3.511.888, 1970.
18. CFR (Compagnie Française de Raffinage), French Patent 2.031.984, 1969.
19. Chevron, US Patent 3.415.737, 1968.
20. Le Page, J. F., "Catalyse de Contact," p. 158, Technip, Paris, 1978.
21. Brunauer, S., Emmett, P. H., and Teller, E., *J. Amer. Chem. Soc.,* **60,** 309 (1938).
22. De Boer, J. H., Linsen, B. G., and Osinga, T. J., *J. Catal.* **4,** 319 (1965).
23. Le Page, J.F., "Catalyse de contact," p. 207, Technip, Paris, 1978.
24. Durand, B., and Nicaise, G., *in* "Kerogen, Insoluble Organic Matter from Sedimentary Rocks," p. 35, Technip, Paris, 1980.
25. Lynch, J. P., Lesage, E., Dexpert, H., and Freund, E., *Inst. Phys. Conf.* **61,** 67 (1981).
26. Boitiaux, J. P., Martino, G., and Montarnal, R., *C.R. Acad. Sci. Paris* **281,** 483 (1975).
27. Franck, J. P., "L'hydrocraquage," Revue IFP, Rueil Malmaison, France, 1978.
28. Ratnasamy, P., and Knozinger, H., *Catal. Rev. Sci. Eng.* **17,** 31 (1978).
29. Trimm, D. L., *in* "Progress in Catalyst Deactivation" (J. L. Figueiredo, Ed.), p. 31, Nijhoff, The Hague, 1982.
30. Burch, R., and Mitchell, A. J., *Appl. Catal.* **6,** 121 (1983).
31. Coughlin, R. W., Kawakami, K., and Hasan, A., *J. Catal.* **88,** 150 (1984).